Grating arrays for high–throughput soft X-ray spectrometers

A. Rasmussen[a] A. Aquila[b] J. Bookbinder[c] C. Chang[d] E. Gullikson[b] R. Heilmann[e]
S. M. Kahn[e] F. Paerels[a] and M. Schattenburg[d]

[a]Columbia Astrophysics Lab, 550 West 120th Street, New York, New York, USA
[b]Center for X-ray Optics, Lawrence Berkeley Lab, Berkeley, CA, USA
[c]Smithsonian Astrophysical Observatory, Cambridge, MA, USA
[d]Space Nanostructures Lab, MIT, Cambridge, MA, USA
[e]Kavli Institute, Stanford University, Palo Alto, CA, USA

ABSTRACT

Cosmic soft X-ray spectroscopy exploits principal transitions of astrophysically abundant elements to infer physical properties of objects in the sky. Most of these transitions, however, fall well below 2 keV, or 6 Angstroms. Consequently, grating spectrometers offer the current, best means by which to analyze soft X-rays from such sources, where throughput and resolving power must be maximized together. We describe grating spectrometer design candidates for the future mission *Constellation–X*, and how the grating array on board (∼1000 gratings in a 1600mm diameter, each for 4 instruments) may be implemented. Grating fabrication and grating alignment approaches require special consideration (over the *XMM-Newton* RGS experience), because of grating replication fidelity and instrument mass constraints.

Keywords: Astrophysical X–ray Spectroscopy, Constellation–X, Reflection Gratings – Arrays

1. INTRODUCTION

The primary goal of this work is to explore instrument performance characteristics for a dispersive grating array optic, to be assembled using identical, flat grating parts.

An example of such an optic has been built and is currently in operation (the RGS grating array aboard *XMM-Newton*[1]). That instrument features 182 large (100×200 mm) grating parts positioned behind each of two XMM mirror module exit apertures, that disperse and collect X-rays in the 5–35Å range. The dispersion angle range subtended by the spectrometer readout ($\sim 2°$), fits a respectable number of spectral resolution elements (~ 600), limited primarily by the moderate angular resolution of the telescopes ($\sim 15''$ HPD).

The large dispersion angles of the *XMM-Newton* RGS are achieved by aligning the gratings (with characteristically "optical" density rulings) at grazing incidence ($\sim 1.58°$), thereby boosting the *projected* ruling density to a large value. Grating diffraction efficiencies are in turn limited by a combination of the graze angles chosen (and the corresponding optical constants) and the projected width of the portion of the groove facet that is illuminated. In general, (ignoring detailed geometry of groove shape for the time being) the width of the illuminated groove facet determines, analogously to single slit illumination, the width and amplitude of the envelope bounding diffracted orders.

Marked similarities in angular resolution of the *Constellation–X* Spectroscopy X-ray Telescope[2] (SXT) to the in-orbit performance of the *XMM-Newton* X-ray Mirror Modules (XMM), have led to similar spectroscopic performances expected for the Con–X RGS in the baseline design.[3] This design features gratings with a maximized diffraction efficiency for a fixed resolving power ($\lambda_B/\Delta\lambda \equiv 400$) at the design (blaze) wavelength of $\lambda_B = 20$Å in first order. The resolving power at λ_B is an input parameter to the grating design, so it can be increased, but at the expense of spectrometer effective area.

Further author information: (Send correspondence to A.R.)
A.R.: E-mail: arasmus@astro.columbia.edu, Telephone: 1 212 854 8126
Address: 550 West 120 Street, New York, NY 10027

Optics for EUV, X-Ray, and Gamma-Ray Astronomy, edited by Oberto Citterio, Stephen L. O'Dell, Proceedings of SPIE Vol. 5168 (SPIE, Bellingham, WA 2004)
0277-786X/04/$15 · doi: 10.1117/12.510045

The possibility was suggested by Cash and then by McEntaffer et al.[4,5] that a different grating design, referred to here as *"off–plane gratings"* (OPG), may offer a substantially greater diffraction efficiency, and if so, a smaller number of gratings could be used to build a spectrometer optic with the same effective area as with the other, *"in–plane grating"* (IPG) design. Furthermore, because of a higher non-vignetting grating packing density, an OPG design would permit strategic placement of the gratings ("sub-aperturing") within the area uniformly populated by gratings in the IPG design.

They went on to suggest an additional key modification in the instrument design that may boost spectral resolving power at the expense of background rejection and source confusion. The idea involves constructing a two dimensional spectroscopic point spread function (PSF) by joining together (figure error dominated) ellipsoidal contributions from each grating or group of gratings. Two closely spaced ($\Delta\lambda$=28mÅ) emission lines could be resolved[5] by eye in most cases. Furthermore, the focal plane can in principle be mapped into dispersion and cross-dispersion components to extract traditional one dimensional spectra.

The remainder of this work is devoted to predicting the performance of the *Constellation-X* RGS. Following a discussion of the two candidate grating geometries and arraying prescriptions, we discuss some new grating efficiency measurement results obtained very recently for candidate IPG and OPG test rulings. The test rulings were fabricated at MIT's Space Nanostructures Laboratory[6,7] and feature atomically smooth groove facets, formed by anisotropically etching off-cut Si wafers. The efficiency testing was performed at beamline 6.3.2[8,9] of the Advanced Light Source (ALS) at Lawrence Berkeley Laboratory. These results are particularly significant because they cover nearly the entire bandpass for *Constellation-X* RGS, for a relevant configuration, in which incidence angles are held fixed to candidate design values. In the subsequent sections, we present detailed design and raytrace results for the two candidate diffraction grating geometries. The discussion includes position and alignment constraints for the gratings across the array, estimates for acceptable misalignments and the resulting spectral resolving power function across the spectrometer readout. We expect these results to help elucidate the requirements and relative benefits of either grating geometry on the way to optimize an ultimate RGS design.

2. DISPERSION GEOMETRY AND ARRAYING PRESCRIPTIONS

To describe the grating dispersion geometry for both IPG and OPG designs, we adopt the following vector equations. Figure 1 provides a reference for the angle definitions (γ, α, β, ψ_i, ψ_f, θ_i and θ_f) used below. It also provides definitions for the mutually orthogonal basis unit vector fields $\hat{n}$, $\hat{r}$ and $\hat{g}$ defined over the grating surface.

In general, the grating array is built so that the focalplane geometry and wavelength scale is identical to that for a *central grating* intercepting light along the *prime ray* at the design angles. Of course, there is not really a grating positioned on the SXT optical axis, since there is no light passing along the prime ray of the SXT – but the central grating is a very useful concept and is used extensively below nevertheless. The focal plane, seen from the central grating, or RGA center, is traced out by the unit vectors $\hat{r_o}$ parallel to $\vec{k_f}$ in a transformed coordinate system where $\vec{k_i}$ is forced parallel to the optical axis ($\hat{z}$):

$$\hat{r_o}\left(m\lambda|d,\theta_i,\psi_i\right) = \begin{pmatrix} \sin\psi_i\cos\left(\theta_i+\theta_f\right)\cos\psi_f + \cos\psi_i\sin\psi_f \\ -\sin\left(\theta_i+\theta_f\right)\cos\psi_f \\ \cos\psi_i\cos\left(\theta_i+\theta_f\right)\cos\psi_f - \sin\psi_i\sin\psi_f \end{pmatrix}, \tag{1}$$

and the central grating normal is given by $\hat{n} = (\cos\theta_i, 0, -\sin\theta_i)$ so that the zero order (specular reflection) solution has zero component in $\hat{y}$. The vectors $\hat{r_o}$ generally trace out a cone, that opens up and becomes a *great circle* as γ, $|\theta_i|$ and $|\theta_f|$ each approach $\pi/2$. In this limit, the dispersion geometry becomes greatly simplified and lends itself to a Rowland Circle construction (e.g., *XMM-Newton* RGS), where it is a relatively simple matter to compute alignment and positioning tolerances and to semi-analytically predict spectrometer spectral performance. In the general (off-plane, conical diffraction) case however, differential forms for the dispersion equation remain fairly complicated and useful semianalytical expressions are elusive. Consequently we rely more heavily on raytraces to estimate the OPG instrument's spectroscopic performance.

In the IPG geometry (cf. Fig. 1 in Ref. 3), the blaze position, where the diffraction efficiency nominally peaks, is used to define the Rowland Circle radius and center by forming an isosceles triangle with vertices

Angle definitions:

$$\gamma \equiv \mathbf{I}\,\mathbf{P}\,\mathrm{gi} = \mathbf{F}\,\mathbf{P}\,\mathrm{gf}$$

$$\psi_i \equiv \mathbf{I}\,\mathbf{P}\,\mathrm{pi};\ \psi_f \equiv \mathbf{F}\,\mathbf{P}\,\mathrm{pf}$$

$$\theta_i \equiv \mathrm{pi}\,\mathbf{P}\,\mathrm{gi};\ \theta_f \equiv \mathrm{pf}\,\mathbf{P}\,\mathrm{gf}$$

$$\tan\theta_{\binom{i}{f}} = \tan\gamma \sin\binom{\alpha}{\beta}$$

$$\sin\psi_{\binom{i}{f}} = \sin\gamma \cos\binom{\alpha}{\beta}$$

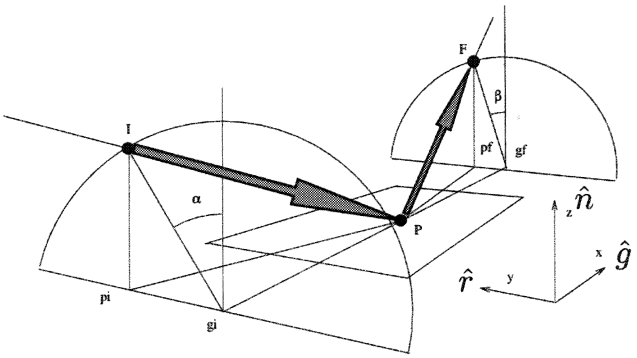

Grating equations:

$$\left|\vec{k_f}\right| = \left|\vec{k_i}\right| \equiv \frac{2\pi}{\lambda}$$

$$\left(\vec{k_f} - \vec{k_i}\right) \cdot \hat{g} = 0$$

$$\left(\vec{k_f} - \vec{k_i}\right) \cdot \hat{r} = \frac{2\pi m}{d}$$

Figure 1. A diagram depicting the generalized dispersion geometry. The local grating basis vectors $\hat{n}$, $\hat{r}$ and $\hat{g}$ and the local groove spacing $d(x,y)$ are defined across the grating surface. Continuous grooves impart an additional equation of constraint (not given here) on $\hat{r}$, $\hat{g}$ and $d(x,y)$.

on the circle, between SXT focus (**F**) – central grating (**G**) – and blaze (**B**). The optimal IPG groove spacing function $d(x,y)$ for the gratings is computed using these positions as parameters, and in the case of *XMM-Newton* RGS, each grating's orientation is computed using points **F** and **B** along with the design angles ψ_i and $\psi_{\mathbf{B}}$. A consequence of this approach is a two dimensionally minimized spot size at **B** and moderate flaring of the spot in the cross-dispersion direction for positions away from **B**.

For the OPG geometry also, we choose a blaze position to form an isoceles triangle **FGB** and compute the ruling density function accordingly. However, if a similar approach is taken to compute individual grating orientations, substantial aberrations in both dimensions are incurred away from **B**, therefore requiring a different alignment scheme.

A second alignment method, applicable for either grating geometry is as follows. This method guarantees a suitably compact zero order spot, crucial for accurate wavelength scale determination. First, the array grating is positioned to deflect the local ray by the included angle by the design value,

$$\Psi = \cos^{-1}\left(\cos\psi_i \cos\left(\theta_i + \theta_f\right)\cos\psi_f - \sin\psi_i \sin\psi_f\right) \tag{2}$$

toward **B**. Second, the grating's normal ($\hat{n}$) vector is computed so that the specularly reflected light will approach the zero order position **M**. Third, the axis of the cone that contains the three points **F**, **M** and **B** (seen from the grating) is computed, and the grating's groove axis vector $\hat{g}$ is made parallel to the cone axis. Finally, the local groove density is "trimmed" by translating the grating in its plane with the local grating vectors $\vec{n}$, $\vec{r}$ and $\vec{g}$ held fixed. This prescription is made with very modest cost in spectral resolution (in the case of IPG arrays), but provides significant improvement in source confusion and background rejection for both designs – also over the *XMM-Newton* RGS in the IPG case.

3. GRATINGS, MEASURED EFFICIENCIES AND SPECTROMETER DESIGN

Grating parameters for the IPG and OPG designs have already been described.[3,5] Meanwhile, the Space Nanostructures Lab (SNL) at MIT has fabricated test rulings that feature atomically smooth groove facets, with parameters close, or similar to, baseline design grating parameters. The in-plane model test ruling dates back to 1997[6] and the off-plane test rulings were fabricated only very recently and are described in more detail in this volume.[7] Together, the gratings represent the first test rulings produced in a similar manner for two candidate grating geometries. Tables 1 and 2 summarize, some baseline spectrometer design constraints and a comparison of the design grating parameters to the actual, fabricated grating parameters.

We report here ALS (synchrotron) measurements of diffraction efficiencies for the MIT fabricated gratings. As mentioned above, they were measured in a relevant configuration, i.e. with angles of incidence fixed, so that

the measured efficiency curves may be applied directly toward an ultimate effective area curve for *Constellation-X* RGS. Because the facility[8,9] is naturally suited to measure reflection and dispersion efficiencies in a plane that includes the incident beam axis, minor modifications were made in fixturing for the sample (grating) and the detector so that the off-plane grating test rulings could be measured. The change in fixturing also forced a change in the normal measurement procedure: The incident beam could not be periodically monitored with the same detector that was used to scan the focalplane, so the incident beam flux was estimated using measurements made earlier or later in the day. The consequence of this is a slightly increased uncertainty in the measured efficiencies, which was still well below the 1% (relative) level. The measured efficiencies, covering most of the RGS instrumental bandpass for the three gratings described in Table 2, are plotted in Figure 2. No attempt is made at this time to electromagnetically model the measured efficiency curves or to infer an effective groove shape given the measured efficiencies. That has been done for other reflection gratings however, with quite reasonable success.[10] Of particular interest, Ref. 11 has provided three dimensional electromagnetic vector calculations to predict spectral order efficiencies for nominal groove shapes for the three MIT test rulings, and these show remarkable resemblance to the efficiency curves shown here. This fact provides additional assurance that grating efficiencies can be modelled reliably given enough detailed information on the average groove shape.

An important point to note on the grating efficiency curves, is that the replica "OPG A" exhibits a well behaved efficiency profile, with its efficiency peaking close to 26Å. The "IPG" on the other hand, shows its efficiency peaking close to 12Å, for a blaze angle characteristic for a much lower density grating (cf. Table 2). A reduction of the groove density from 580 mm^{-1} to 407 mm^{-1} would typically result in the curve shifting toward the right by 40% in wavelength, a moderate increase in peak efficiency and a slight narrowing of the efficiency profile. Likewise, a 16% increase in groove density for the "OPGs" would result in a moderate shift toward shorter wavelength of the peak, accompanied by a peak reduction and broadening out of the efficiency profile.

For the purpose of instrument modelling, we will not attempt to *correct* these measured efficiency curves to approximate hypothetical efficiencies for gratings meeting the design specifications. Instead, we will use the grating groove densities of the test rulings measured here, so that the efficiency curves and spectral resolving powers are self consistent. It is important to be aware, however, that tradeoffs between spectral resolution and spectral efficiencies exist for IPG and OPG alike.

Table 1. Summary of the design parameters that describe an RGS aboard *Constellation-X*.

Spectrometer feed	F/6 nested foil, 1600 mm OD (SXT) 10000 mm focal length, 15 arcsecond (HPD) ~ 50% aperture interception by gratings
Number of gratings	~1000 per array (~100 identical sub–assembly modules of ~10 gratings each)
Gratings	Size: ~ 200 × 100 mm Flatness: ≤ 2 arcsecond non-flatness (HEW), freestanding Production: directly fabricated (anisotropically etched off–cut Si wafer) or step–and–flash nano–imprint replication onto flat glass
Dispersion angles	Limited by graze angle (γ) that provides high reflectivities over the passband (<4° for Au)
Resolving power	Limited by SXT optic, providing ~240 resolving power per degree dispersion angle
Spectrometer readout	Focal Plane Array of back–illuminated X–ray CCDs with "event drive" charge detection circuitry for low power, high framerate operation

4. RAYTRACES AND SPECTRAL PERFORMANCE

Full raytracing was used to verify and assess the arraying prescriptions and resulting optical characteristics of the *Constellation-X* RGS, for both IPG and OPG geometries. This approach in estimating instrument performance is necessary in part, because of the complex nature of the OPG geometry, but also provides a means to estimate how

Table 2. Summary of the grating parameters for the IPG and OPG designs, along with parameters for the fabricated test rulings. The "resolution element" ($\Delta\lambda$) row is included, assuming **G** is 9365 mm from **F** and neglectinge contributions from grating misalignments and aberrations induced by finite grating size. A more detailed assessment of the spectral performance is given in § 4.3. Some improvements in $\Delta\lambda$ are made with subaperturing and with two dimensional PSF construction, as described in §1 and demonstrated in §4.4.

	IPG		OPG		
Parameter	Design	test ruling "IPG"	Design	test ruling "OPG 40"	test ruling "OPG A"
ruling density $1/d$ (mm^{-1})	407	580	5800	5000	5000
cone angle γ	90°	90°	2.0°	1.84°	2.0°
"tilt" incidence α	88.39°	88.39°	30°	20°	30°
incidence angle ψ_i	1.61°	1.61°	1.73°	1.73°	1.73°
blaze δ	0.605°	0.7°	11°	7.0°	7.0°
graze angle on facet (incident and at blaze)	2.215°	2.31°	1.89°	1.79°	1.84°
exit angle at blaze ψ_B	2.82°	3.01°	1.98°	1.83°	1.92°
wavelength at blaze (Å)	20.0	17.0	21.7	15.3	15.7
blaze wavelength for arraying (Å)	NA	20	NA	NA	20
resolution element $\Delta\lambda$ at 20Å per 15″ SXT (mÅ)	54	38	134	155	155

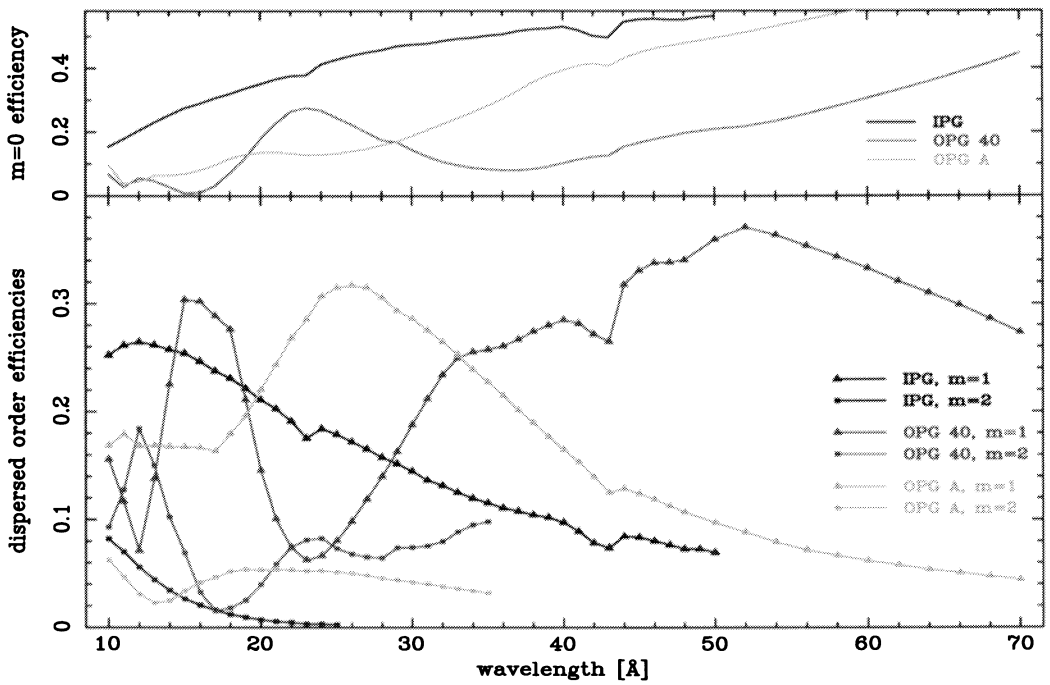

Figure 2. Measured grating efficiencies for three types of gratings fabricated at the MIT SNL. The parameters for the gratings are given in Table 1. The efficiency curves for specular reflection (m=0) in the top tier and dispersed spectral order efficiencies (m=1,2) in the bottom tier. The features seen close to 23 and 43 Å are due photoelectric absorption by contaminants, which are presumably hydrocarbons or esters. The wavelength sampling used (1Å steps) was insufficient to adequately sample real modulations in order efficiencies for the "OPG 40" test ruling. The remarkable difference between "OPG 40" and "OPG A" efficiency curves is due to the change in grating groove shape, since "OPG A" is a replica pulled from a master grating very similar to "OPG 40" and is essentially a *negative* of the master. Micrograph images for "OPG 40" and "OPG A" are given in Fig. 6 and Fig. 8 of Heilmann et al.[7] (this volume). (this volume) respectively.

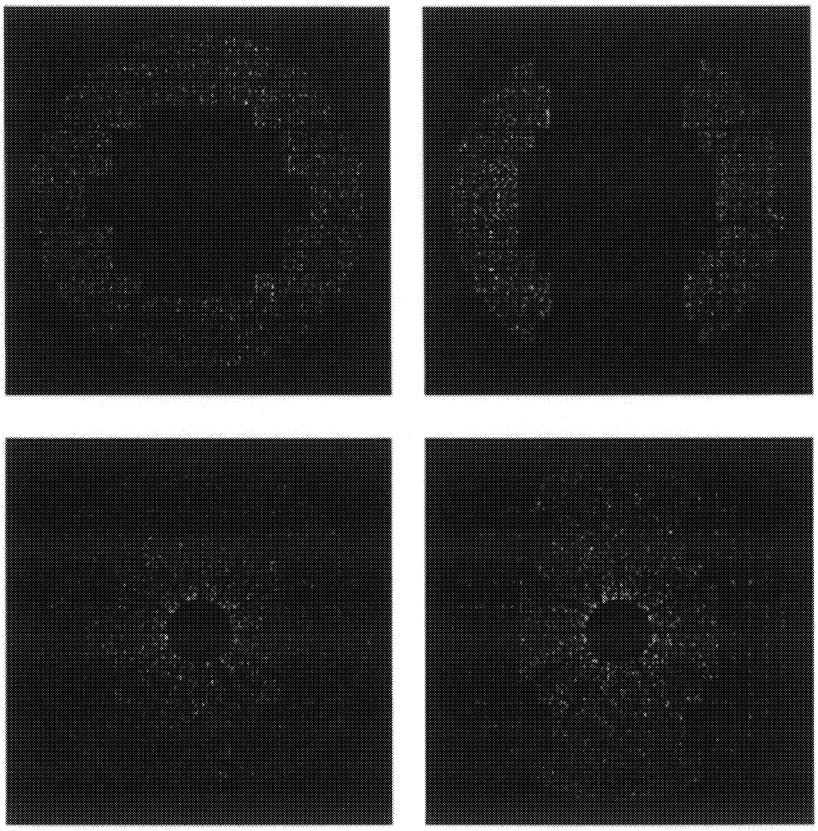

Figure 3. A graphic representation showing the distribution of gratings in the SXT exit aperture. Left: the IPG model; Right: the OPG model. The top row displays the distribution of light that is intercepted by the gratings (for each model), while the bottom row shows the distribution of light passing on toward the SXT prime focus (microcalorimeter) instrument. The fraction of light intercepted by gratings in the IPG model is within ~6% of that for the OPG model. This *subaperturing* of the OPG gratings improves the spectral resolution element over the approximate value given in Table 2. The grating normals face the right.

the six possible misalignments (about $\hat{n}$, $\hat{r}$ and $\hat{g}$) and mispositionings (in $\hat{n}$, $\hat{r}$ and $\hat{g}$) of each grating contribute to degrading the spectral resolution from that expected solely by the SXT contribution. Further, the benefits of subaperturing gratings in the array and shaping a two dimensional PSF (in the OPG model) are typically highly dependent on how the SXT error budget is balanced between figure errors and sagittal positioning of the shells,[12] so different assumptions are readily tested. Aberrations induced by using ***flight size*** gratings and the same grating design throughout the array are also easily estimated by simply changing the size of the grating model, with each grating center positioned optimally.

One major shortcoming of the current modelling effort is that aberrations induced by the *modular design* of the grating array, i.e. using identical grating subassembly modules to form the overall grating array is not computed yet, since in the arraying scheme, each grating is positioned independently in the software. These aberrations, and designs for an optimal grating subassembly module will be deferred for now. We continue to compute the grating array's contribution to the spectral resolution element $\Delta\lambda_{HEW}$, for both the IPG and OPG approaches.

4.1. A Provisional SXT Model

Three nested foil, Wolter I SXT raytrace models were used to illuminate the grating arrays, each comprised of 143 paraboloid-hyperbloid pairs. The first was a "perfect" model, without figure errors or coaxial misalignments.

The resulting PSF at focus had widths of 0.2 and 0.4″ in measures of linear FWHM and HEW, respectively and 0.8″ in HPD – which provides verification of the raytrace surface interception and deflection routines. The second and third SXT models each have a 15″ HPD, but with different relative contributions from shell figure errors and mirror segment sagittal misalignments: The second SXT model has no contribution from misalignments, but with figure errors corresponding to 4″ (1σ) at each surface. Finally, the third SXT model has 150μm (1σ) sagittal shell misalignments and 3.4″ (1σ) figure errors on each surface. While the HPD figures match for these two SXT models (and thereby meet the SXT requirement of 15″), the linear FWHM values are 4.1 and 12.4″, respectively – the latter model broadened substantially by finite sagittal misalignments.

4.2. The RGS Grating Arrays

Figure 3 illustrates the interception of the SXT exit aperture by the two grating arrays. As described previously, the IPG array covers the full outer annulus with an interception factor of roughly 60%, while the OPG covers a 60% fraction of the outer annulus with 100% local interception by the grating modules.

Each grating array contains 1056 gratings of the size specified in Table 1, nominally housed in 96 subassemblies of 11 each. However, the OPG model subassemblies are about 60% smaller, due to their higher packing density permitted by the OPG geometry.

4.3. Image Formation, Astigmatism and Background Rejection

In the raytrace, photons missing the gratings are discarded, while the ones intercepted by gratings are dispersed according to the wavelength and the order selection used. An appropriate focal surface is chosen, that minimizes the spot size in the dispersion direction. Figure 4 shows results (for IPG and OPG models) of the focal plane search for both dispersion and cross–dispersion axes. A mismatch in the best focus position in the dispersion and cross-dispersion axes indicates an astigmatic image formation. The astigmatism is reduced substantially by using the *conical diffraction* arraying prescription described in § 2 above. The resulting monochromatic spotsize image areas are also given as a function of dispersion coordinate, which indicates a significant improvement in background rejection for the IPG design over the RGS aboard *XMM-Newton*. The plots indicate that except for at the shortest wavelengths, the IPG image areas are smaller than those for the OPG, typically by at least 30 or 40%.

The full end-to-end resolving power function $\lambda/\Delta\lambda_{HEW}$, plotted as a function of dispersion coordinate is given in Figure 5. In performing the calculations for the OPG design, we note an aberration that contributes to the resolution element function that scales with the grating *width*, which is nominally 100 mm. This aberration becomes insignificant when a much larger number of gratings are used in the raytrace, or when each grating is given a "chirp" or a ruling density gradient component parallel to the $\hat{r}$ vector, and where the chirp is dependent on the grating's position in the array. Figure 6 shows the contribution of this aberration for these various grating options. The aberration is also more thoroughly discussed in § 4.4.

4.4. A 2–D PSF for the OPG Array

Following earlier demonstrations by Cash et al (ref), we used the raytrace and a focalplane mapping algorithm to narrow down the effective spectrometer PSF, by forming a two dimensional PSF at the blaze positon. This was achieved by aligning each grating to an offset blaze positon ($\mathbf{B}_{off}$) according to the azimuthal angle of the grating. Figure 7 shows the raytrace results of this process, and the results of the focalplane mapping operation. We see that the nominal random misalignments tolerated for the IPG model are apparently insufficient to form a well behaved, easily mapped two dimensional PSF, *even at blaze!* More specifically, control of the OPG's rotation about its normal ($\hat{n}$) would need to be held to much tighter tolerances than the current value of 2 arcminutes (FWHM). This is somewhat ironic because the presence or absence of the same misalignments had negligible effect on the resolving power curves computed for OPGs, shown in Figure 5.

The requirements for improving the OPG resolving power over the curves given in Figure 5 are far reaching indeed.

First, it would appear that with basleine RGS grating array description (~1000 identical gratings) it will be impossible to form a resolution element $\Delta\lambda_{HEW}$ smaller than ~34mÅ*: Either many more, smaller grating parts

*This estimate was made using the first SXT model (a "perfect telescope) and 100 × 200 mm gratings.

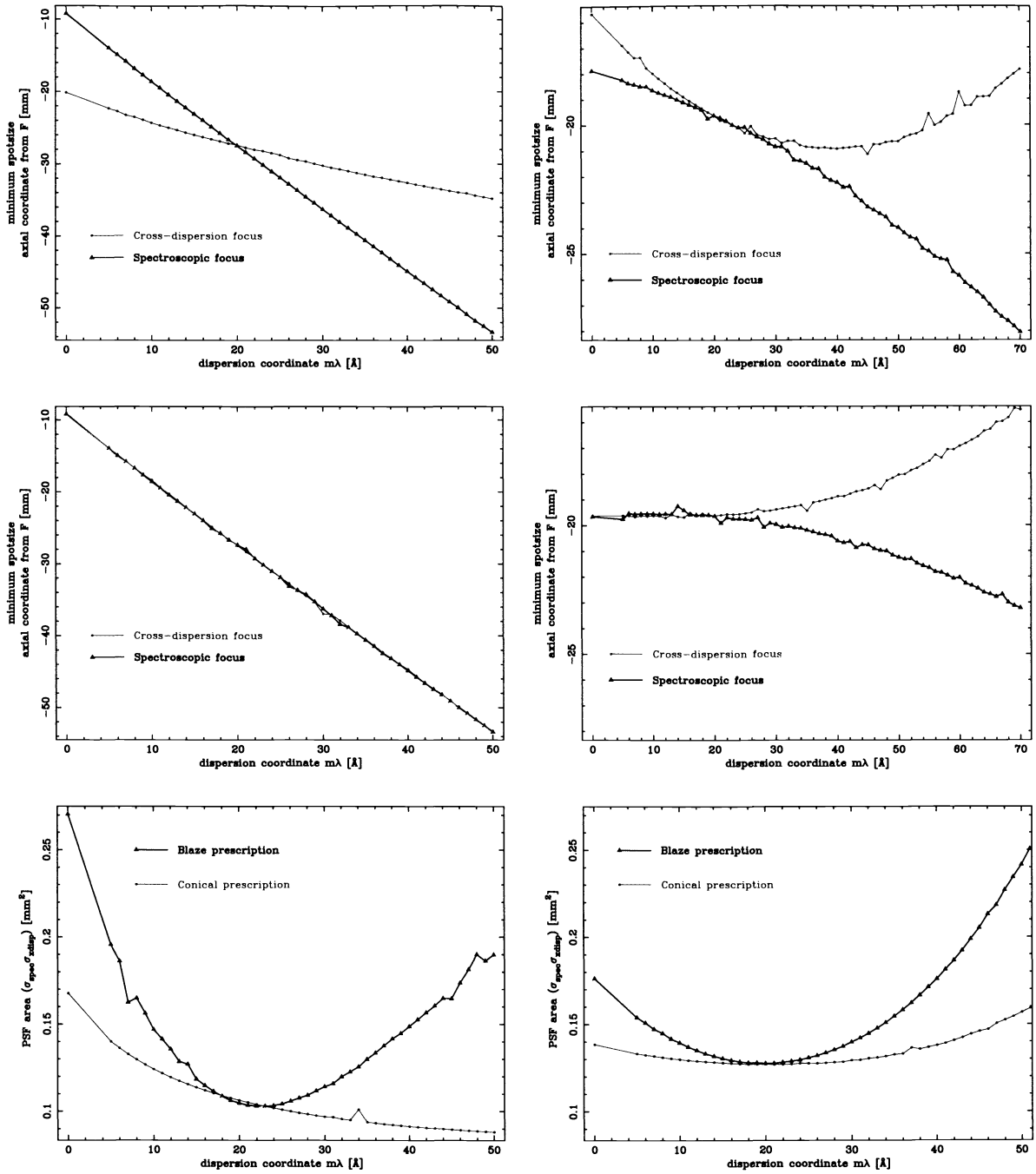

Figure 4. Astigmatism of the RGS grating arrays for the IPG (left) and OPG (right) geometries. Using only the points **F** and **B** (at 20Å) and the combination of design angles at each grating center, the astigmatism is significant for positions away from blaze. By using the prescriptions described in § 2 (middle plots), the astigmatism problem is reduced significantly, almost entirely in the IPG case. Changes in the monochromatic PSF area (in terms of $\sigma_{disp} \times \sigma_{x-disp}$) are plotted on the bottom. This reduction in spot area corresponds to a benefit for background rejection as well as source confusion.

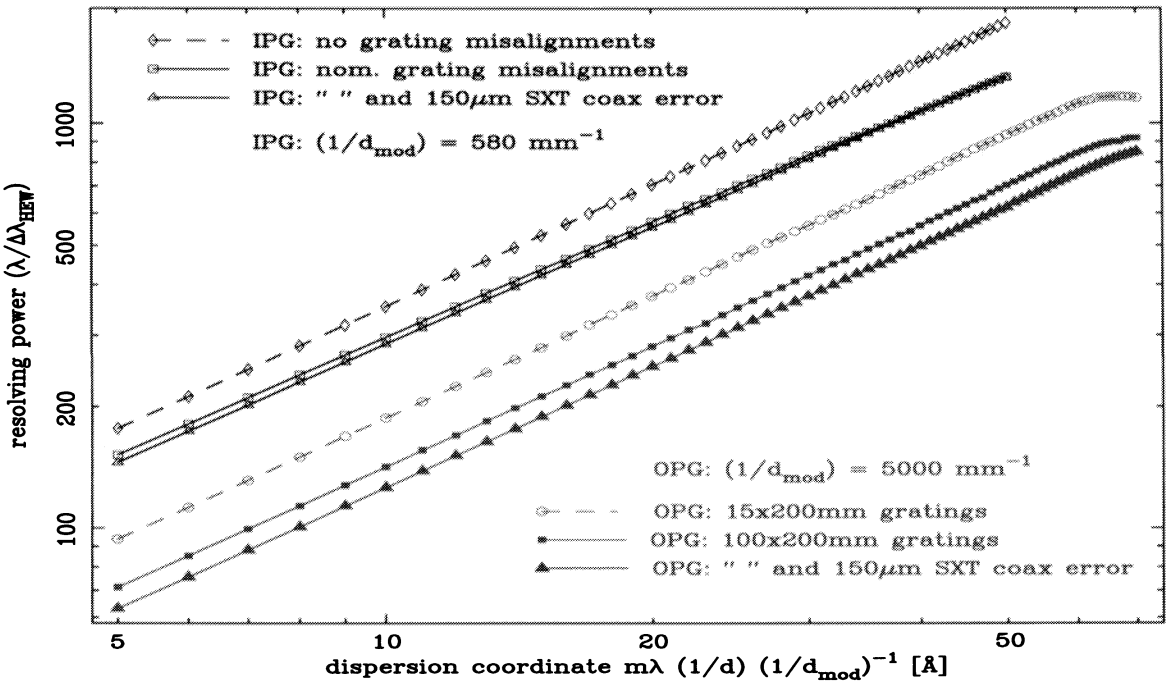

Figure 5. The resolving power, defined as $\lambda/\Delta\lambda_{HEW}$, measured from the raytrace runs. The focal plane for the OPG case was taken from the measured spectral focal surface shown in the central right plot of Figure 4. The budgeted grating misalignments (dominated by 2″ FWHM terms in both grating flatness and grating alignment) are responsible for the drop in IPG resolving power from the top to the lower two IPG curves. The same nominal grating misalignments were used for the OPG raytraces, but there, resolution element ($\Delta\lambda_{HEW}$) there is dominated by the aberration mentioned above, which scales with grating width. An additional degradation is imparted to the OPG resolving power by a sagittal SXT optic co-location error of 150μm (using the third SXT model described above), which corresponds to 3″ (1σ) at the focal plane. The end result of this comparison shows a factor of 2.5 or so higher resolving power for the IPG RGA over the OPG RGA, based on parameters of the test rulings measured (§ 3).

(~6400) would be needed per array, or several, position specific grating models (each with a different chirp in addition to the radial grooves) would need to be fabricated and then assembled only in the specific locations. Either approach would be a substantial and possibly costly, turn from the current baseline.

Second, tightening the alignment tolerances about the grating normal $\hat{n}$ to permit PSF shaping and remapping is probably feasible but would require special consideration in the assembly process that would probably include additional precise reference surfaces or fiducials on each grating. However, unless the baseline description is modified to circumvent the aberration problem, only moderate improvements will be possible with this technique.

Third, even if the two preceding problems are partially solved to improve the potential resolving power for the OPG array, the details of the SXT alignment may ultimately limit the effectiveness of those improvements. As noted above, a 150μm (1σ) sagittal mirror shell co-location error, well below the SXT mirror 15″ HPD requirement, will place a lower limit on the spectral resolution element $\Delta\lambda_{HEW}$ of 44mÅ for an 5000 mm^{-1} OPG array, on par with the lowest (580 mm^{-1}) IPG performance shown in Figure 5.

5. CONCLUSIONS

We have presented here the first "representative" effective area curves for candidate grating test rulings for the *Constellation-X* reflection grating spectrometer. The high quality grating test rulings represent each of two possible grating geometry designs, here referred to the in-plane and off-plane gratings (IPG and OPG, respectively). We also determined and used some arraying prescriptions that were applicable to both IPG and

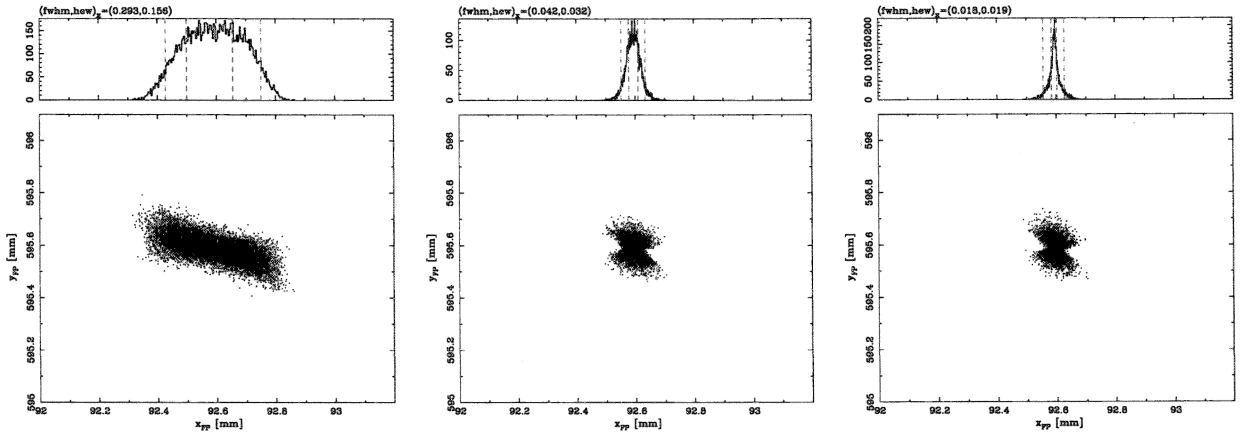

Figure 6. Examples on how to reduce the grating size induced aberration. These raytraces were performed using the "perfect" mirror (first SXT model) and perfectly aligned gratings for clarity and to demonstrate the lower limit to the spectral resolution element. Left: The dispersed spot at blaze for 100×200 mm gratings. Center: Same as the left, but with grating size 15×200 mm. Right: 100×200 mm gratings, but the gratings now have a *chirp* that depends on the grating's position in the array. The chirps used here vary the ruling density by ±0.19% across the 100 mm grating width, with the chirp sense alternating between the "north" and "south" subapertures. The the nominal $\Delta\lambda_{HEW}$ (using the second SXT model) decreases from 71 to 54 to 58mÅ for the these calculations, respectively. Using the third SXT model, from 80 to 71 to 73mÅ, respectively.

OPG array designs. Raytrace simulations were made to generate predictions of the spectral performance for each candidate array, as if each were populated with flight gratings identical to the test ruling gratings. In the case of the IPG array, these predictions, combined with the measured efficiency, form a computational RGS that has moderately higher spectral resolution, and moderately lower effective area, than an array built using baseline gratings. Attempts to improve the (superior efficiency) OPG array spectral resolution proved possible, but would require substantial changes in the baseline array description, in-plane grating alignment tolerances, and would impose additional requirements on the internal structure of the feeding SXT optic.

ACKNOWLEDGMENTS

We acknowledge many useful discussions with Webster Cash, Randy McEntaffer, Ann Shipley and Steve Osterman, all of the University of Colorado, that helped to formulate some of the questions attempted to answer here. The work at Columbia was supported by NASA. MS, RH, CC and grating fabrication work was supported by NASA grant NAG5-12583. The work at the LBNL was supported by the Office of Energy Research, Basic Energy Sciences, of the U. S. Department of Energy under contract No. DE-AC03-76SF00098.

REFERENCES

1. J. W. den Herder, A. C. Brinkman, S. M. Kahn, G. Branduardi-Raymont, K. Thomsen, H. Aarts, M. Audard, J. V. Bixler, A. J. den Boggende, J. Cottam, T. Decker, L. Dubbeldam, C. Erd, H. Goulooze, M. Güdel, P. Guttridge, C. J. Hailey, K. A. Janabi, J. S. Kaastra, P. A. J. de Korte, B. J. van Leeuwen, C. Mauche, A. J. McCalden, R. Mewe, A. Naber, F. B. Paerels, J. R. Peterson, A. P. Rasmussen, K. Rees, I. Sakelliou, M. Sako, J. Spodek, M. Stern, T. Tamura, J. Tandy, C. P. de Vries, S. Welch, and A. Zehnder, "The Reflection Grating Spectrometer on board XMM-Newton," **365**, pp. L7–L17, Jan. 2001.
2. R. Petre, W. W. Zhang, D. A. Content, T. T. Saha, J. Stewart, J. H. Hair, D. Nguyen, W. A. Podgorski, W. R. Davis, M. D. Freeman, L. M. Cohen, M. L. Schattenburg, R. K. Heilmann, Y. Sun, and C. R. Forest, "Constellation-X spectroscopy X-ray telescope (SXT)," in *X-Ray and Gamma-Ray Telescopes and Instruments for Astronomy. Edited by Joachim E. Truemper, Harvey D. Tananbaum. Proceedings of the SPIE, Volume 4851, pp. 433-440 (2003).*, pp. 433–440, Mar. 2003.

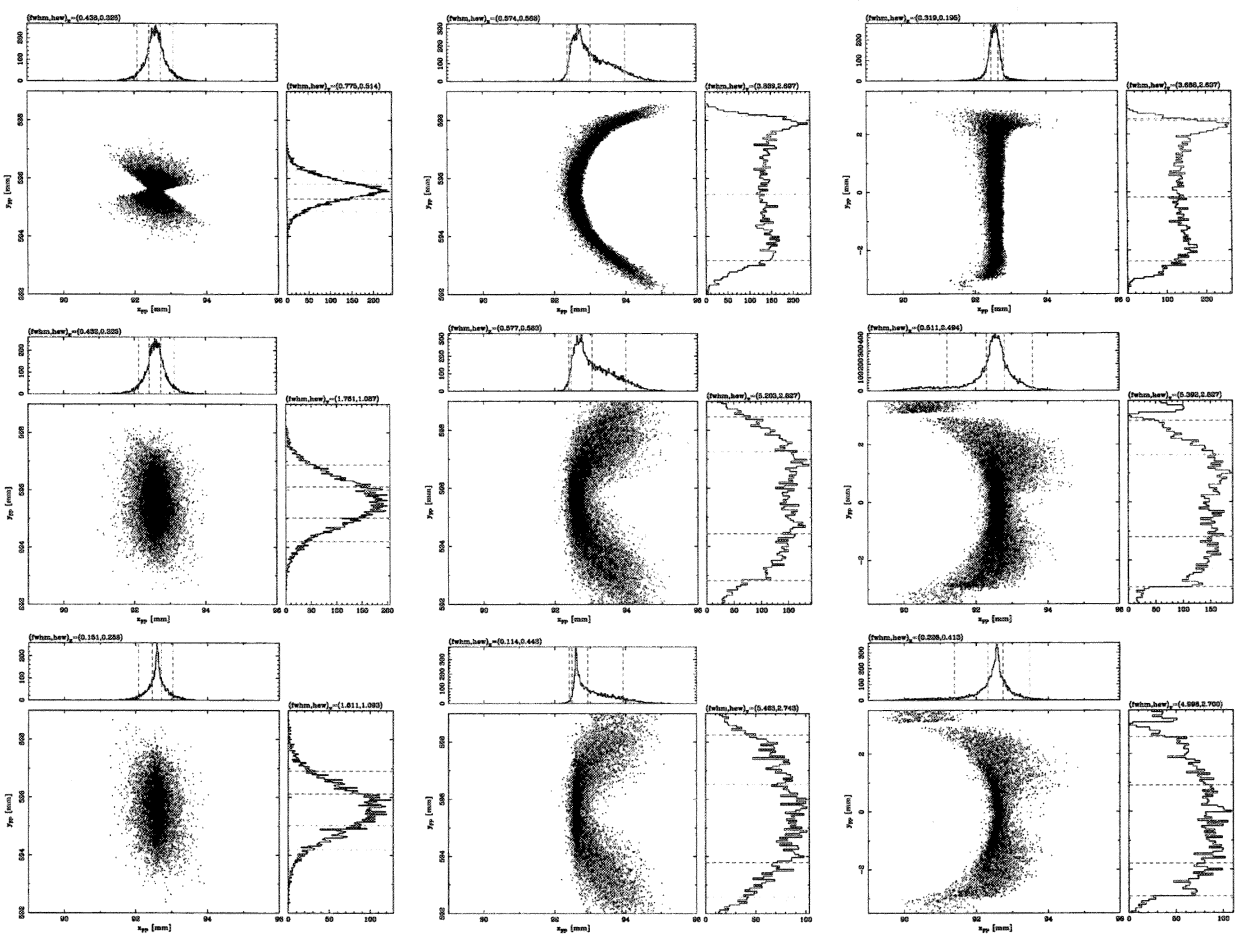

Figure 7. A demonstration of how a two dimensional image can be built and then mapped to recover, in some cases, significant spectral resolving power. To produce these calculations we have used an SXT with figure errors only (second SXT model). Each row of plots shows the same sequence, i.e. Left: image formation at blaze (**B**) without the two dimensional prescription applied; Center: individual gratings have been tipped according to their azimuthal coordinate, to form circular segment with radius 3 mm. Right: the same data as in the center, but now mapped into dispersion and cross-dispersion coordinates. The top row shows the calculation results for a grating array with no alignment errors, for clarity. There, the excercise has decreased the spectral resolution element size ($\Delta\lambda_{HEW}$) by 40%, from 71 to 42mÅ. The second row shows results for a grating array with the nominal misalignment distribution used for the IPG models, i.e. FWHM measures of $2''$ in flatness, $2''$ in alignment about $\hat{r}$, $4''$ about $\hat{g}$ and $2'$ about the grating normal $\hat{n}$. In this case the attempt to improve spectral resolution fails, and the spectral resolution element (HEW) increases from 71 to 108mÅ. Finally, the bottom row shows results for a grating array with the same, nominal misalignment distribution but built out of narrow gratings, containing approximately 6400 per array. The aforementioned aberration is less dominant in the resolution element (56mÅ). As seen in the middle case, the improvement fails, with the resolution element degrading to 90mÅ.

3. S. M. Kahn, F. B. Paerels, J. R. Peterson, A. P. Rasmussen, M. L. Schattenburg, G. R. Ricker, M. W. Bautz, J. P. Doty, G. Y. Prigozhin, J. A. Nousek, D. N. Burrows, J. E. Hill, and W. C. Cash, "Large-area reflection grating spectrometer for the Constellation-X mission," in *Proc. SPIE Vol. 3765, p. 94-103, EUV, X-Ray, and Gamma-Ray Instrumentation for Astronomy X, Oswald H. Siegmund; Kathryn A. Flanagan; Eds.*, pp. 94–103, Oct. 1999.
4. W. C. Cash, "X-ray optics. II - A technique for high resolution spectroscopy," **30**, pp. 1749–1759, May 1991.
5. R. L. McEntaffer, W. C. Cash, and A. F. Shipley, "Off-plane gratings for Constellation-X," in *X-Ray and Gamma-Ray Telescopes and Instruments for Astronomy. Edited by Joachim E. Truemper, Harvey D. Tananbaum. Proceedings of the SPIE, Volume 4851, pp. 549-556 (2003).*, pp. 549–556, Mar. 2003.
6. A. E. Franke, M. L. Schattenburg, E. M. Gullikson, J. Cottam, S. M. Kahn, and A. Rasmussen, "Super-smooth x-ray reflection grating fabrication," *Journal of Vacuum Science & Technology B: Microelectronics and Nanometer Structures, Volume 15, Issue 6, November 1997, pp.2940-2945* **15**, pp. 2940–2945, Nov. 1997.
7. R. K. Heilmann, M. Akilian, C. H. Chang, C. G. Chen, C. R. Forest, C. Joo, P. T. Konkola, J. C. Montoya, J. Sun, and M. L. Schattenburg, "Advances in reflection grating technology for Constellation-X," in *Optics for EUV, X-Ray and Gamma-Ray Astronomy. Edited by O. Citterio and S. L. O'Dell. Proceedings of the SPIE, Volume 5168, (these proceedings)*,
8. J. H. Underwood, E. M. Gullikson, M. Koike, P. J. Batson, P. E. Denham, K. D. Franck, R. E. Tackaberry, and W. F. Steele, "Calibration and standards beamline 6.3.2 at the Advanced Light Source," *Review of Scientific Instruments* **67**, pp. 3372–+, Sept. 1996.
9. E. M. Gullikson, S. Mrowka, and B. B. Kaufmann, "Recent developments in EUV reflectometry at the Advanced Light Source," in *Proc. SPIE Vol. 4343, p. 363-373, Emerging Lithographic Technologies V, Elizabeth A. Dobisz; Ed.*, pp. 363–373, Aug. 2001.
10. J. W. den Herder, A. C. Brinkman, S. M. Kahn, G. Branduardi-Raymont, M. Audard, E. Behar, A. Blustin, A. J. F. den Boggende, J. Cottam, C. Erd, C. Gabriel, M. Guedel, K. van der Heyden, J. S. Kaastra, A. Kinkhabwala, M. A. Leutenegger, R. Mewe, F. B. S. Paerels, A. J. J. Raassen, J. R. Peterson, A. Pollock, A. P. Rasmussen, M. Sako, M. Santos-Lleo, K. Steenbrugge, T. Tamura, and C. P. de Vries, "Performance and results of the reflection grating spectrometers onboard XMM-Newton," in *X-Ray and Gamma-Ray Telescopes and Instruments for Astronomy. Edited by Joachim E. Truemper, Harvey D. Tananbaum. Proceedings of the SPIE, Volume 4851, pp. 196-207 (2003).*, pp. 196–207, Mar. 2003.
11. L. I. Goray, "Rigorous efficiency calculations for blazed gratings working in in– and of–plane mountings in the 5–50Å wavelengths range," in *Optics for EUV, X-Ray and Gamma-Ray Astronomy. Edited by O. Citterio and S. L. O'Dell. Proceedings of the SPIE, Volume 5168, (these proceedings)*,
12. W. A. Podgorski and J. Bookbinder, "Constellation-X spectroscopy x-ray telescope image error budget and performance prediction," in *Optics for EUV, X-Ray and Gamma-Ray Astronomy. Edited by O. Citterio and S. L. O'Dell. Proceedings of the SPIE, Volume 5168, (these proceedings)*,